Conversion of SO_2 to SO_3 by In Situ Photolysis of SO_2 and O_3 Mixtures Isolated in Argon Matrixes: Isotopic Effects†

H. Chaabouni, L. Schriver-Mazzuoli,* and A. Schriver

Laboratoire de Physique Moléculaire et Applications, Laboratoire Associé à l'Université Pierre et Marie Curie, Unité Propre du CNRS, Université Pierre et Marie Curie, Tour 13, Case 76, 4 Place Jussieu, 75252 Paris Cedex 05, France

Received: September 8, 1999; In Final Form: December 13, 1999

The mechanism of photooxidation of sulfur dioxide in the presence of ozone and under irradiation at 266 nm has been investigated at low temperature in an argon matrix. Formation of stable SO_3 occurs from the reaction between SO_2 and $O(^1D)$ and also by oxygen atom transfer within the SO_2:O_3 complex. Use of isotopic SO_2 species led to unusual observations suggesting that photooxidation of SO_2 proceeds via an intermediate species, namely, OSOO; this trioxide sulfur isomer transforms into SO_3 by tunneling. In the gas phase, the quenching of the $O(^1D)$ atom by SO_2 could occur through this intermediate.

1. Introduction

One of the major channels for the formation of sulfuric acid aerosols in the troposphere involves oxidation of SO_2 in the gas and/or liquid phase or on solid surfaces. A large number of models and mechanisms have been proposed.[1−5] Direct oxidation of excited sulfur dioxide molecules by oxygen was found to be nonexistent, but formation of sulfur trioxide was observed through photolysis of molecular donor−acceptor complexes. As an example, the dimeric species $(SO_2)_2$ can be readily photooxidized after irradiation in the 230−410 nm range in sulfur trioxide in an oxygen matrix at 12 K.[6] A similar observation was reported in the photolysis of the SO_2:CH_2O complex isolated in oxygen matrix.[7] Ten years ago, as part of studies on the mechanism of H_2SO_4 formation, we reported on the formation (in argon matrix) of SO_3 by photolysis of the O_3:SO_2 complex with a 90-W medium-pressure mercury lamp.[8] We have initiated recently new studies with ^{18}O-enriched ozone and ^{18}O-enriched sulfur dioxide to identify spectroscopically the product SO_3 and its isotopic variants. Unexpected observations led us to investigate in detail photolytic processes involving ^{18}O-containing species using laser irradiation at 266 nm.

In this paper, we will first describe the infrared spectrum of the SO_2:O_3 complex, and then we will present the results of photolysis studies of the SO_2/O_3 system at 266 nm performed in argon matrix. Contrary to previous studies,[6] the reaction of SO_2 with $O(^1D)$ was shown to be effective. On the basis of these experimental observations, a mechanism is proposed.

In the lower atmosphere, ozone is known to play a major role in the oxidation of SO_2. In tropospheric clouds (weak acidic environment), oxidation of SO_2 by ozone was shown to be of importance.[9] In the gas phase, oxidation occurs mainly through the reaction of SO_2 with the OH radical, which is a secondary product of ozone photolysis.[10,11]

2. Experimental Section

The cryogenic system used in the present studies consisted of a rotatable closed cycle refrigerator (Air Product Displex 202 A) with KBr optical windows for performing IR reflection measurements and one quartz window for ultraviolet photolysis. Mixtures of gaseous reagents were deposited at 20 K onto a gold-plated mirror at a rate of 10^{-2} mol/h. A temperature controller (silicon diode 9600-1) was used to maintain the chosen temperature to within ±0.1 K. Ozone was prepared from natural oxygen (Air Liquide N50) and from isotopic $^{18}O_2$ (Eurisotop CEA) contained in a glass vacuum finger excited by a Tesla coil discharge, trapping ozone at liquid-nitrogen temperature. Residual oxygen was removed by freeze−pump−thaw cycles using liquid nitrogen. Unfortunately, during the preparation of ozone, we are not able to eliminate completely impurities such as CO_2 and SiF_4. Weak absorption bands assigned to SiF_4 were measured at 1027.5 and 1023.1 cm^{-1}. Natural sulfur dioxide (Air Liquide N30) was dried over P_2O_5 and distilled at low temperature. ^{18}O-Enriched sulfur dioxide was prepared from natural sulfur (Prolabo) and ^{18}O-enriched oxygen (Eurisotope, 98% ^{18}O) through the combustion reaction $S + O_2 \rightarrow SO_2$. Argon (Air Liquide N56) was used as carrier gas without further purification. Gas mixtures were prepared by standard manometric techniques on grease-free vacuum lines. Spectra were recorded with a FTIR Bruker IFS 113 v spectrometer in the reflection mode at a nominal resolution of 0.1 cm^{-1}. The optical path between the beam extractor and the cryostat was nitrogen-purged to avoid atmospheric absorption by CO_2 and H_2O. Photodissociation was carried out at 266 nm using the fourth harmonic of a Nd-YAG laser (YG 781C-20 from Quantel), which operates at 20 Hz with 4-ns pulse duration. The light intensity was spatially homogenized with a divergent lens placed in front of the UV window of the cryostat. The fluence inside the cryostat was estimated from the power measured with a detector PSV 3102 Gentec S/N 61592 with a section of 1.76 cm^2 that was placed after the lens and a CaF_2 window of the same material as the entrance window of the cryostat.

3. Results and Discussion

To simplify the rather cumbersome full isotopic notation, we will use simplified conventions with, for example, $^{16}O_3$ for $^{16}O^{16}O^{16}O$, $^{18}O_3$ for $^{18}O^{18}O^{18}O$, $S^{16}O_2$ for $^{16}OS^{16}O$, and $S^{18}O_2$ for $^{18}OS^{18}O$.

† Part of the special issue "Marilyn Jacox Festschrift".

* To whom correspondence should be addressed.

10.1021/jp993164e CCC: $19.00
Published on Web 02/26/2000

TABLE 1: Frequencies (cm^{-1}) of Ozone Monomers Containing ^{16}O and ^{18}O Trapped in Argon (from Ref 12) and of Sulfur Dioxide Monomers Containing ^{16}O and ^{18}O in Stable (S) and Metastable (M) Sites in Argon Matrix (from Ref 17)

	ν_1 (cm^{-1})		ν_2 (cm^{-1})		ν_3 (cm^{-1})	
$^{16}O_3$	1105.1[b]	1105.2[a]	703.6[b]	704.2	1039.7[b]	1041.2
$^{16}O^{16}O^{18}O$	1090.1[b]	1091.7	687.2[b]	687.9	1025.8[b]	1027.3
$^{18}O^{16}O^{18}O$	1071.5[a,b]	1072.9[a]	670.6[b]	671.8	1016.8[b]	1018.4
$^{16}O^{18}O^{16}O$	1074.5[a,b]	1076.1[a]	696.0[b]	696.6	1006.3[b]	1007.7
$^{18}O^{18}O^{16}O$	1060.3[b]	1062.2	680.0[b]	680.8	991.8[b]	993.2
$^{18}O_3$	1040.4[a,b]	1041.9[a]	663.4[a,b]	664.3[a]	982.5[b]	984.0

	ν_1 (cm^{-1})		ν_2 (cm^{-1})		ν_3 (cm^{-1})	
	S	M	S	M	S	M
$S^{16}O_2$	1152.3[b]	1147.2	519.9	517.3[b]	1355.5	1351.3[b]
	1151.7			516.9	1355.0[b]	1350.9
$^{16}OS^{18}O$	1124.4[b]	1119.7[b]	509.2	506.8	1336.3	1332.4
	1123.8	1119.4			1335.9[b]	1332.0[b]
$S^{18}O_2$	1101.7[b]	1096.9	498.8	496.0[b]	1312.0	1308.0[b]
	1101.2			495.6	1311.5[b]	1307.7

[a] Calculated values. [b] Strongest component of the doublet.

3.1. Vibrational Spectra and Photodissociation at 266 nm of Parent Molecules. *3.1.1. Ozone Molecule in Ar.* Infrared spectra of natural and isotopic ozone in argon are well-documented.[12] In this matrix, all the fundamental bands appear as doublets pertaining to ozone in a single or a double site.[13] Table 1 recalls the fundamental frequencies of ozone monomers containing ^{16}O and ^{18}O isotopes.

At 266 nm, ozone photolysis produces mainly the oxygen atom in the first excited state (85%).[14] In the argon matrix, the $O(^1D)$ atom is efficiently quenched by argon atoms at the production site, and most of the resulting $O(^3P)$ atoms recombine with molecular oxygen to reform ozone. However, the observed small decrease of ozone absorption peaks is due to cage escape of oxygen atoms, a process that is dependent on temperature and on photon flux.[15,16]

3.1.2. Dioxide Sulfur Molecule in Ar. Infrared spectra of the different isotopic species of the SO_2 monomer trapped in an argon matrix have been previously reported.[17] As for ozone, doublets are observed in each fundamental region assigned to SO_2 molecules trapped in stable and metastable sites. With increasing temperature, the low wavenumber peak of the doublet (characterizing the metastable site) decreases and disappears above 33 K. Table 1 recalls the fundamental frequencies of sulfur dioxide-containing ^{16}O and ^{18}O isotopes.

Recently, an isomer of dioxide sulfur, namely, sulfur peroxide (SOO), was identified spectroscopically by Chen et al.[18] It was formed by irradiation of SO_2 isolated in an argon matrix with light at 193 nm.

Sulfur dioxide dissociates into SO + O only below 218 nm, but SO_2 absorbs strongly in the 240−330 nm region with a much weaker absorption from 340 to 400 nm, and electronically excited states can be produced.[19] The strong absorption system leads to two singlet states of SO_2, while the weak absorption populates a triplet state:

$$SO_2(X^1A_1) + h\nu \xrightarrow{240 < \lambda < 330\ nm} SO_2(^1A_2, ^1B_2)$$

$$SO_2(X^1A_1) + h\nu \xrightarrow{340 < \lambda < 400\ nm} SO_2(^3B_1)$$

In gas phase, the excited singlet states of SO_2 can be quenched by other molecules into the $^3B_1$ triplet state, which is subsequently relaxing to the ground electronic state. Formation of SO_3 from reaction of this triplet state with SO_2 or O_2 has also been suggested.[20,21]

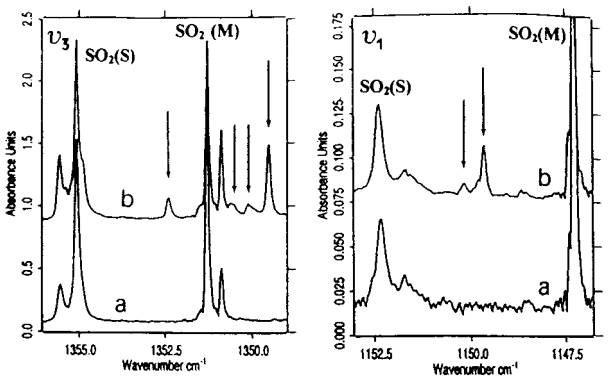

Figure 1. Infrared spectra of SO_2 in the ν_3 and ν_1 regions. New features arising from the co-deposition of SO_2 with O_3 in an argon matrix (trace b) compared to a blank experiment with SO_2 in argon only (trace a). Spectra are recorded at 11 K after deposition at 20 K. (a) $S^{16}O_2/Ar$ = 1/2000. (b) $S^{16}O_2/^{16}O_3/Ar$ = 1/4/2000. New bands are marked by arrows. S and M, stable and metastable sites for SO_2.

3.2. Identification of the O_3:SO_2 Complex in Ar. *3.2.1. Regions of the SO_2 Fundamentals.* As shown in Figure 1, the spectrum of $S^{16}O_2$ in argon co-deposited with O_3 (typically $SO_2/O_3/Ar$ = 1/4/2000) exhibits two new distinct bands in the ν_3 region. They are located at 1352.4 and 1349.5 cm^{-1}, the latter being the most intense ($I_{1352.4}/I_{1349.5}$ = 0.35/1). Note in Figure 1 the appearance of two other very weak features at 1350.6 and 1350.1 cm^{-1} which were not observed in the spectra of the parent molecules. Because of their weakness, they are not further considered in this work. To determine if the two bands at 1352.4 and 1349.5 cm^{-1} both belong to a 1:1 complex between $S^{16}O_2$ and O_3, several experiments were carried out with various relative concentrations of $S^{16}O_2$ and O_3. Results showed that, in all the experiments, the two bands maintained a constant intensity ratio. Furthermore, after the annealing at 35 K (leading to the disappearance of the metastable site features of $S^{16}O_2$), the two new bands diminished in intensity but kept the same relative intensity ratio. Consequently, the two features were assigned to a 1:1 $S^{16}O_2$:O_3 complex. This multiplicity could be due either to matrix site effects (trapping of the complex in two matrix cages of different geometries) or to the existence of two conformers of similar stability. In the ν_1 region of $S^{16}O_2$, a weak doublet was also observed at 1150.2−1149.6 cm^{-1} (Figure 1) and was assigned to the same 1:1 complex. In the ν_2 region, the bands of the complex were too weak to be observed.

The decrease in the frequency of the ν_1 and ν_3 bands for the strongest component of the complex $S^{16}O_2$:O_3, calculated with respect to the stable (S) monomer bands, is 2.7 and 5.6 cm^{-1}, respectively, showing that the antisymmetric ν_3 mode is the most sensitive to perturbations as previously reported for other complexes formed between SO_2 and H_2O,[22] NH_3,[23] HNO_3,[24] and $(CH_2SH)_2$.[25] The observed red shift of the ν_3 mode of $S^{16}O_2$ in the complex with O_3 is smaller than the red shift observed for the sulfur dioxide dimer ($\Delta\nu$ = 13.8 cm^{-1})[17] and for the $S^{16}O_2$:H_2O complex ($\Delta\nu$ = 11.8 cm^{-1}) in an argon matrix.[22] The relative intensity of the ν_3 and ν_1 absorptions in the complex does not change substantially as compared to the SO_2 monomer in the stable site (ν_3/ν_1 = 14.3), indicating that the weak interaction between sulfur dioxide and ozone involves a negligible charge transfer and is mainly due to dipole−quadrupole or dipole-induced−dipole interactions.

Mixed isotopic sulfur dioxide SO_2 in argon was also co-condensed with the O_3/Ar mixture. Figure 2 shows a typical

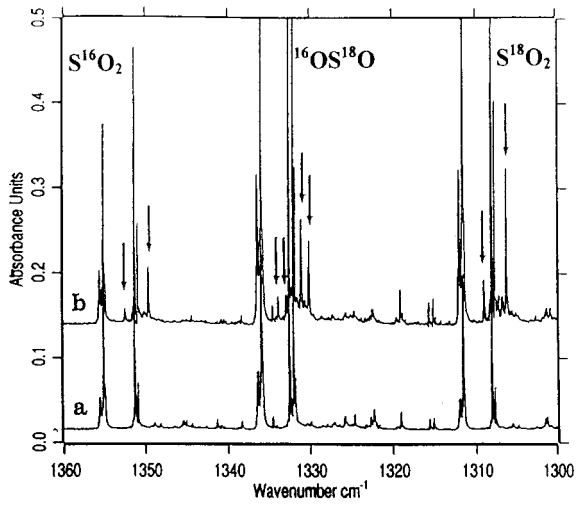

Figure 2. Infrared spectra of SO_2 in the ν_3 region. New features arising from the co-deposition of mixed isotopic SO_2 species with natural ozone in an argon matrix (trace b) compared to a blank experiment of mixed SO_2 isotopic species only in argon (trace a). Spectra are recorded at 11 K after deposition at 20 K. (a) $S^{16}O_2$, $^{16}OS^{18}O$, $S^{18}O_2$/Ar = 1/3000. (b) $S^{16}O_2$, $^{16}OS^{18}O$, $S^{18}O_2/^{16}O_3$/Ar = 1/6/3000. New bands are marked by arrows.

TABLE 2: Observed Frequencies (cm^{-1}) for $S^{16}O_2$, $^{16}OS^{18}O$, and $S^{18}O_2$ Involved in a 1:1 Complex with O_3

	species			
	$S^{16}O_2$:O_3		$^{16}OS^{18}O$:O_3	$S^{18}O_2$:O_3
modes	ν (cm^{-1})	(*A*)	ν (cm^{-1})	ν (cm^{-1})
ν_3	1352.4	(0.35)	1333.8	1309.0
			1332.8	
	1349.5	(1)	1331.0	1306.2
			1330.0	
ν_1	1150.2	(0.01)	1122.2	
	1149.6	(0.07)	1121.4	1099.2

[a] Relative band intensities (*A*) are indicated in parentheses.

spectrum in the ν_3 region recorded at 11 K after deposition. In addition to the doublet observed for the $S^{16}O_2$ sample, two new lines were noticeable at 1309.0−1306.2 cm^{-1} on the low wavenumber side of the $S^{18}O_2$ monomers, and two pairs of lines of equal intensities were observed on the low wavenumber side of the $^{16}OS^{18}O$ monomers at 1333.8−1332.8 and 1331.0−1330.0 cm^{-1}. The presence of four features assigned to the two $^{16}OS^{18}O$:O_3 complexes is the indication of the nonequivalence of the two SO oscillators in the complex.

Table 2 summarizes the characteristic frequencies of the SO_2 submolecule in the complex with ozone.

3.2.2. Regions of the Ozone Fundamentals. As compared to pure ozone, the presence of SO_2 induces a new weak satellite band in the ν_3 ozone spectral region. It is measured at 1039.8 cm^{-1} as a shoulder on the high-frequency side of the ν_3 band of the ozone monomer in the double site. With scrambled isotopic ozone, six absorptions noted with arrows in Figure 3 were observed at 1039.8, 1026.0, 1017.0, 1006.3, 991.9, and 982.6 cm^{-1}. They showed the same relative intensities as in pure ozone, but the features corresponding to unsymmetrical isotopic ozone species were broader than those corresponding to symmetrical species as presented with scale expansion in Figure 3 for the ν_3 mode ozone 666 and ozone 668. As explained in ref 26, in a complex in which the ozone submolecule keeps the same symmetry (C_{2v}) as ozone itself, a sextet that matches the intensity distribution of the monomer isotopic ozone bands is expected. In the case of asymmetric ozone complexes due to a terminal oxygen attachment, a multiplet with eight components of equal intensity in the ν_3 ozone region is expected. If we assume that the ozone band has the same full-width half-maximum for all isotopic species, our observations seem to indicate that the SO_2:O_3 complex is probably asymmetric with the existence of two overlapped satellite bands for the unsymmetrical 668 and 886 species of ozone.

The weak blue shift ($\Delta\nu$ = 0.26 cm^{-1}) observed for the ν_3 mode frequency from monomer to complexed ozone is again the indication of a weak interaction between SO_2 and O_3, weaker than that in the H_2O:O_3 complex for which a blue shift of ozone monomer band was found to be 3.3 cm^{-1}.[27]

3.3. Photolysis of Natural $S^{16}O_2/^{16}O_3$/Ar Mixtures. Most of the experiments were performed at 11 K with mixtures in argon containing 1/10 000 of $S^{16}O_2$ and 1/1000 of $^{16}O_3$ to minimize the formation of the dimer $(SO_2)_2$ and to increase the yield of the complex $S^{16}O_2$:$^{16}O_3$. In some experiments, irradiation was carried out after matrix annealing to eliminate $S^{16}O_2$ in metastable sites.

Irradiation with the 266-nm laser line caused the disappearance of the complex. A weak decrease in intensity of both forms of the sulfur dioxide monomer (but more effective for SO_2 in metastable sites) was also observed. The evolution of SO_2 depends on the initial ozone concentration and on the irradiation power as well as on the temperature, as discussed below. In parallel, a triplet located at 1392.2, 1391.7, and 1391.5 cm^{-1} is appearing with a weak feature close to the $S^{16}O_2$ monomer observed at 1353.6 cm^{-1} with a satellite at 1353.1 cm^{-1}. The triplet absorption was assigned to the formation of sulfur trioxide despite the difference in the spectrum in the ν_3 region of $S^{666}O_3$ deposited directly in argon. In the argon matrix, the ν_3 mode of SO_3 monomer is characterized by a doublet at 1385.1 and 1388.8 cm^{-1} due to site splitting.[28] In a recent paper[29] concerning the infrared matrix isolation study of H_2SO_4 and its complexes with H_2O, bands at 1392.4 and 1396 cm^{-1} were observed and assigned to the ν_3 mode of SO_3 perturbed by several H_2O neighbors. In the present matrix study, only traces of water are present, and as previously reported,[8] the 1:1 H_2O:SO_3 complex is not formed in the argon matrix. Thus, the 6-cm^{-1} blue shift observed after photolysis is probably due to the perturbation of the produced SO_3 molecule by the other photoproduct of the reaction produced at the same site, namely, the O_2 molecule.

Absorption at 1353.6 cm^{-1}, which appeared below the $S^{16}O_2$ monomer in a stable site, was assigned to $S^{16}O_2$ produced in another site through the reaction between $S^{16}O_2$ and $O(^1D)$ regenerating SO_2. As previously observed in other photolysis experiments,[30,31] products after photolysis in a site containing the reactants are expected to exhibit a small shift as compared to the same products when they are directly and/or separately deposited.

In some experiments, a prolongated photolysis (during 40 min) was performed after disappearance of the complex. As illustrated in Figure 4, the absorption by $S^{666}O_3$ increased after the disappearance of the $S^{16}O_2$:O_3 complex. This behavior was enhanced when photolysis was performed at 20 K instead of at 11 K. As illustrated in Figure 5, at this temperature the complex disappears rapidly, and the formation of SO_3 is correlated to the decrease of SO_2. An asymptotic limit is reached when ozone is totally depleted. The 1352.4 cm^{-1} feature also showed the same behavior. These observations are the indication that SO_3 formation has two origins: the first one is due to the reaction within the complex, and the second one is due to the reaction of excited atomic oxygen with SO_2. This latter reaction depends on ozone photodissociation, and the increase in ozone concen-

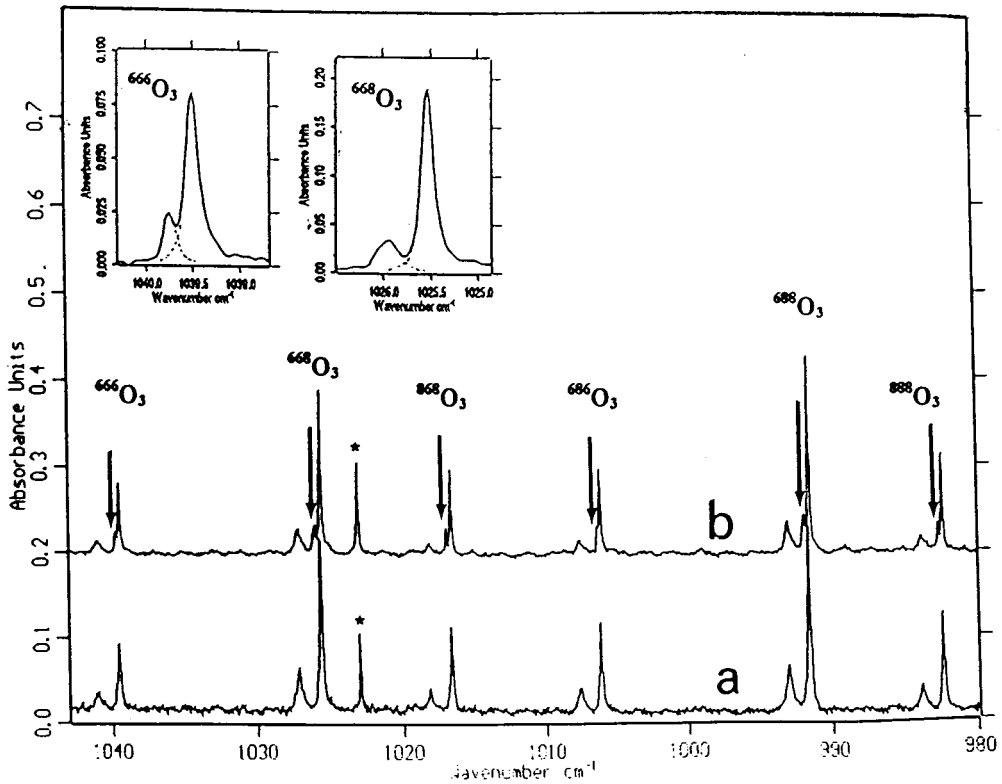

Figure 3. Comparison in the ν_3 region of ozone of infrared spectra recorded at 11 K of (a) argon matrix containing scrambled isotopic ozone (O_3/Ar = 1/4000) and (b) argon matrix containing scrambled isotopic ozone and natural sulfur dioxide (SO_2/O_3/Ar = 1/2/4000). New bands are marked by arrows, and a zoom is presented around the features of normal ozone and unsymmetrical ^{18}O ozone demonstrating the larger width of the new feature in the latter case. *, impurity.

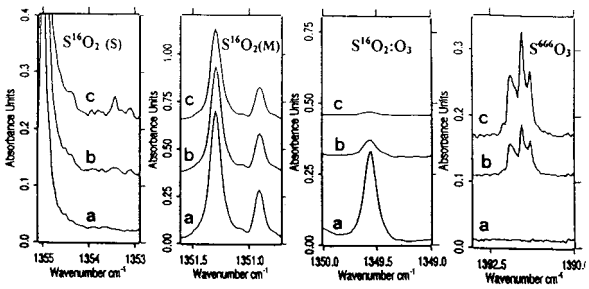

Figure 4. Evolution of the spectrum of a $S^{16}O_2/^{16}O_3$/Ar sample (1/3/3000) as a function of irradiation time (with a 266-nm laser line) in the 1355−1353, 1351.5−1350.5, 1350−1349, and 1393−1390 cm^{-1} spectral regions. Irradiation time: (a) t = 0, 6, and 45 min. Photon flux = 4.2 × 10^{16} photons cm^{-2} s^{-1}.

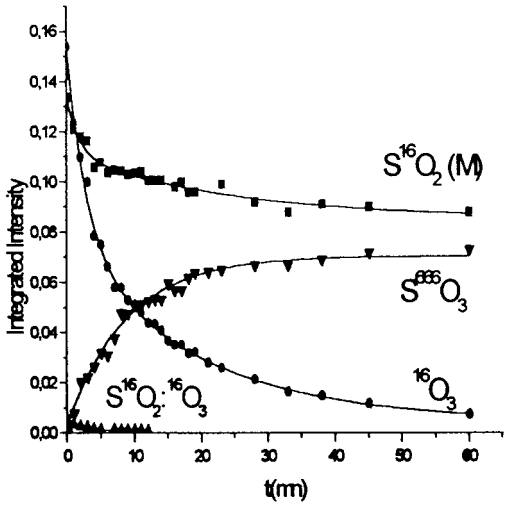

Figure 5. Integrated intensity versus photolysis time showing the SO_3 (≈1391 cm^{-1} triplet) growth, O_3 (1039.8 cm^{-1}) decay, metastable SO_2 (1351 cm^{-1} doublet) decay, and SO_2:O_3 (1349.7 cm^{-1}) decay in argon matrix. (SO_2/O_3/Ar = 1/3/3000). The photolysis was performed at 20 K with the 266-nm laser line. Photon flux = 4.2 × 10^{16} photons cm^{-2} s^{-1}.

tration favors this pathway, while an increase in temperature favors the exit rate of oxygen atom, another channel to enhance production of SO_3.[16] After annealing of the photolyzed matrix, which allows diffusion of atomic oxygen and relaxation to its ground state, no change was observed, indicating that ground-state oxygen atoms were not reactive in absence of irradiation. The ratio of the final ν_3 absorbance of $S^{666}O_3$ species appearing after irradiation and the sum of the ν_3 bands of $S^{16}O_2$ in both sites and of $S^{16}O_2$ complexed by ozone both disappearing under irradiation was measured. It was found equal to 1.5 instead of 1 for the ratio of the two absorbances as measured in the gas phase on a molecule per molecule basis.[32] This difference can be due to a matrix effect or more probably to an absorbance coefficient difference between SO_3 directly deposited and SO_3 in a cage with a O_2 molecule.

Kinetic studies of the disappearance of the $S^{16}O_2$:$^{16}O_3$ complex were also carried out. The decrease in the concentration of the complex was followed by the decrease of the integrated intensity (A) of the SO_2 absorption peak at 1349.5 cm^{-1}. Plots of ln (A^0/A^t) versus irradiation times were observed to be linear, indicating that the photolysis of the complex can be considered as a first-order process (A^0 is the initial integrated intensity of the ν_3 SO_2 absorption in the complex, and A^t is the intensity at current irradiation time, t). For a typical irradiation experiment (F = (4.2 ± 0.4) × 10^{16} photons cm^{-2} s^{-1}), an apparent constant rate of (4.2 ± 0.5) × 10^{-3} s^{-1} was measured. Unfortunately, in the absence of absolute absorption cross section values for the

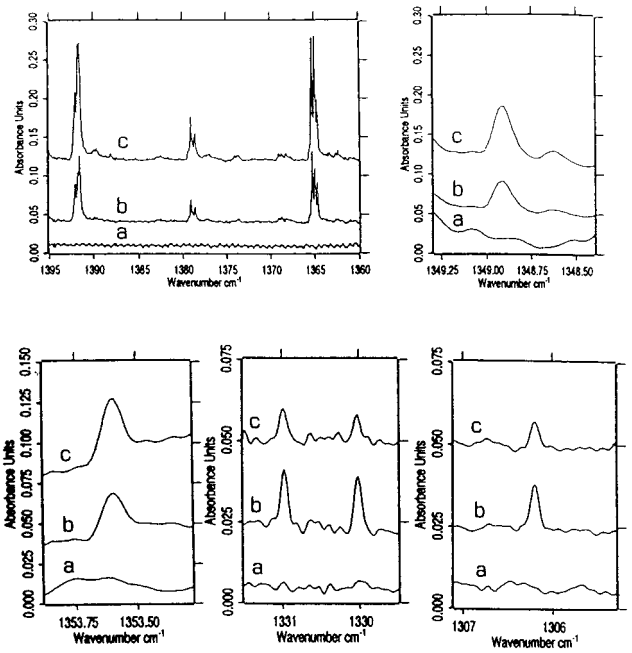

Figure 6. Growth of product bands during laser photolysis of a $S^{16}O_2/^{18}O_3$/Ar (1/4/4000) mixture in typical spectral regions (see text). Photolysis time: (a) 0, (b) 10, and (c) 40 min.

complex, it was impossible to calculate the quantum yield of the photolytic process.

To check if the formation of SO_3 was also a first-order process, the experimental results were analyzed with the following equation pertaining to the growth (see Figure 5) of a product formed in a first-order process:

$$[SO_3]^t = [SO_3]^\infty[1 - \exp(-kt)] \text{ or}$$

$$\ln [(A^\infty_{SO_3} - A^t_{SO_3})/A^\infty_{SO_3}] = -kt$$

where t is the current irradiation time, and ∞ refers to the value obtained after the disappearance of ozone. The plot of $\ln [(A^\infty_{SO_3} - A^t_{SO_3})/A^\infty_{SO_3}]$ versus the irradiation time for the same experiment gave a nearly straight line with a slope of about $(2.0 \pm 0.5) \times 10^{-3}$ s^{-1}.

Note that after long photolysis, characteristic bands of SO_4 appeared at 1443.1−1442.9 and 1272.9 cm^{-1}.[33] Formation of SO_4 (which is not the subject of this work) is due to the subsequent reaction of SO_3 with atomic oxygen.

3.4. Photolysis of $S^{16}O_2/^{18}O_3$/Ar Mixtures. The same photolysis experiments as above were performed with a mixture of natural $S^{16}O_2$ and $^{18}O_3$ in an argon matrix with a photon flux of 4.2×10^{16} photons cm^{-2} s^{-1}. As previously noted, the characteristic bands of the $S^{16}O_2$:O_3 complex and $S^{16}O_2$ monomer diminished. The complex disappears rapidly after 10 min of irradiation with approximately the same first-order apparent constant as previously measured with normal ozone for the same irradiation power. Figure 6 illustrates the growth of the new features observed with heavy ozone for different irradiation times, and Table 3 lists the observed frequencies. In the ν_3 region of SO_3, two triplets of comparable overall intensity were observed at 1392.0_5−1391.7−1391.5 cm^{-1} and at 1365.0−1364.9−1364.7 cm^{-1} with in addition a weak triplet at 1379.1−1378.8−1378.6 cm^{-1}. They increased upon prolonged irradiation until the disappearance of ozone. In the ν_3 region of $S^{16}O_2$, the 1353.6 cm^{-1} band previously observed in the photolysis of natural $S^{16}O_2 + {}^{16}O_3$ mixtures and assigned to $S^{16}O_2$ was again present. New features at 1334.3, 1331.0−1330.0, 1310.1−1309.1, and 1306.2 cm^{-1} were also observed. The 1331.0−1330.0 cm^{-1} doublet and the 1306.2 cm^{-1} band disappeared upon photolysis as shown in Figure 6.

Appearance of two relatively intense triplets in the ν_3 region of SO_3 is the indication of the formation of $S^{668}O_3$, and the observation of a weak triplet at 1379.1−1378.8−1378.6 cm^{-1}, which is correlated to the 1348.9 cm^{-1} feature, is the indication of the formation of $S^{688}O_3$ in a weaker yield. In the $S^{668}O_3$ and $S^{688}O_3$ species, the symmetry is C_{2v}, and the ν_3 (E′) band of $S^{666}O_3$ (symmetry D_{3h}) splits into two bands of symmetry A_1 and B_2. These frequencies are in agreement with those reported in ref 6. The higher frequency triplet of $S^{668}O_3$ is close to the ν_3 band of the $S^{666}O_3$ species. However, on the basis of equal intensity of the bands characterizing $S^{668}O_3$, it can be assumed that only $S^{668}O_3$ is formed without $S^{666}O_3$ species. The ν_1 mode of $S^{668}O_3$ is active and could have been observed. However, no band corresponding to this mode was observed probably due to its weakness and to the small yield of the photoproduct. Doublets at 1331.0−1330.0 cm^{-1} and at 1306.2 cm^{-1} have been assigned in section 3 to $^{16}OS^{18}O$:O_3 and $S^{18}O_2$:O_3 complexes, respectively. Very weak bands at 1334.3 and 1310.1−1309.1 cm^{-1} observed as blends near the $^{16}OS^{18}O$ and $S^{18}O_2$ monomers were assigned to the isotopic SO_2 monomer regenerated in a different site as discussed above.

Note that in the ν_3 region of O_3, weak bands at 1025 and 1006 cm^{-1} characteristic of $^{16}O^{16}O^{18}O$ and $^{16}O^{18}O^{16}O$ species appeared after irradiation. However, their yield was variable with the initial ozone concentration; hence, they were not produced in the reaction of SO_2 with atomic oxygen as confirmed by a blank experiment corresponding to irradiation of a binary sample $^{18}O_3$/Ar in the same experimental conditions. They are probably due to dissociation with a low yield of initial $^{16}O^{18}O^{18}O$ and $^{18}O^{16}O^{18}O$ present in the concentrated $^{18}O_3$ species followed by the recombination of O_2 and O according to

$$^{16}O^{18}O^{18}O \rightarrow {}^{16}O + {}^{18}O_2$$

$$^{18}O + {}^{16}O^{18}O$$

$$^{16}O + {}^{16}O^{18}O \rightarrow {}^{16}O^{16}O^{18}O \text{ and } {}^{16}O^{18}O^{16}O$$

3.5. Photolysis of Mixed $S^{16}O_2$, $^{16}OS^{18}O$, and $S^{18}O_2$ Species Co-Deposited with $^{16}O_3$ and $^{18}O_3$ in Argon. Two sets of experiments were performed with a mixed isotopic SO_2 mixture containing $S^{16}O_2/^{16}OS^{18}O/S^{18}O_2$ in a 1/2.5/2 proportion. In the first set, the SO_2 mixture was co-deposited with $^{16}O_3$, and in the second set, it was co-deposited with $^{18}O_3$. In both cases, irradiation at 266 nm was performed with a photon flux of 1.14×10^{16} photons cm^{-2} s^{-1}, smaller than in previous experiments.

For the first mixture (with $^{16}O_3$), we might anticipate finding bands for $S^{666}O_3$, $S^{668}O_3$, and $S^{688}O_3$, and for the second mixture (with $^{8}O_3$), we would expect to find bands for $S^{668}O_3$, $S^{688}O_3$, and $S^{888}O_3$. The notation is used to exemplify the oxygen isotopes in SO_3 but is not providing details on the exact geometry (planar anyway). As illustrated in Figure 7 in the three ν_3 SO_3 isotopic regions, these bands were observed.

For the first set of experiments, the 1392.2−1391.8−1391.5 cm^{-1} triplet is about twice as intense as the 1365.3−1364.9−1364.7 cm^{-1} triplet because it corresponds to a mixture of $S^{666}O_3$ and $S^{668}O_3$, whereas triplets of equal intensity at 1379.1−1378.9−1378.6 and 1349.4_5−1349.1−1348.9 cm^{-1} characterizing $S^{886}O_3$ are observed. For the second set of experiments, the later triplet is more intense than the triplet at 1379.0−1378.8−1378.6 cm^{-1} because it corresponds to a mixture of $S^{888}O_3$ and $S^{688}O_3$.

TABLE 3: Infrared Frequencies (cm^{-1}) of Major Products Observed following Photolysis of Samples of Isotopic SO_2 and O_3 Isolated in Solid Argon

$S^{16}O_2/^{16}O_3$/Ar ν (cm^{-1})	$S^{16}O_2/^{18}O_3$/Ar ν (cm^{-1})	$S^{16}O_2$, $^{16}OS^{18}O$, $S^{18}O_2/^{16}O_3$/Ar ν (cm^{-1})	$S^{16}O_2$,$^{16}OS^{18}O$, $S^{18}O_2/^{18}O_3$/Ar ν (cm^{-1})	attribution[a]
1443.1−1442.9		1443.2−1443.0		$S^{6666}O_4$
		1424.3		$S^{6668}O_4$*
	1423.3	1423.3	1423.3	$S^{6688}O_4$*
	1422.7		1422.6	$S^{6888}O_4$*
			1398.6	$S^{8888}O_4$
1392.2−1391.7−1391.5		1392.2−1391.8−1391.5		$S^{666}O_3(\nu_3)$
	1392.0_5−1391.7−1391.5	1392.0_5 −1391.8−1391.5	1392.0−1391.7−1391.5	$S^{668}O_3(\nu_3)$
	1379.1−1378.8−1378.6	1379.1−1378.9−1378.6	1379.0−1378.8−1378.6	$S^{688}O_3(\nu_3)$
	1365.0−1364.9−1364.7	1365.3−1364.9−1364.7	1365.2−1364.9−1364.6	$S^{668}O_3(\nu_3)$
1353.6−1353.1	1353.6−1353.1	1353.6−1353.1	1353.6−1353.0	$S^{16}O_2$
		1349.5		$S^{16}O_2$:O_3
	1348.9	1349.4_5−1349.1−1348.9	1349.4_5−1349.1−1348.9	$S^{688}O_3(\nu_3)$
			1349.3−1348.9−1348.6	$S^{888}O_3(\nu_3)$
	1334.3	1334.3	1334.3	$^{16}OS^{18}O$
	1331.0−1330.0	1331.0−1330.0	1331.0−1330.0	$^{16}OS^{18}O$:O_3
	1310.1−1309.1	1310.1−1309.7	1310.1−1309.9	$S^{18}O_2$
	1306.2		1306.2	$S^{18}O_2$:O_3
1272.9		1272.9		$S^{6666}O_4$
		1247.3		$S^{6668}O_4$*
	1242.6	1242.5	1242.5_5	$S^{6688}O_4$*
	1226.9		1226.9	$S^{6888}O_4$ *
			1224.8	$S^{8888}O_4$

[a] An asterisk indicates tentative attribution.

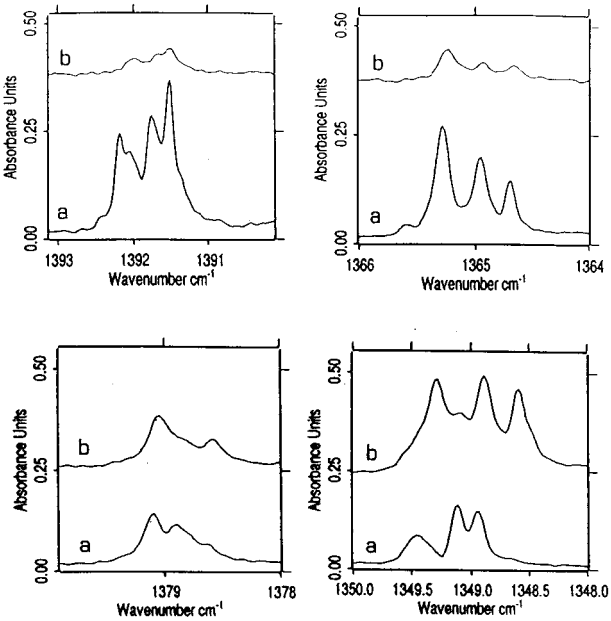

Figure 7. Comparison in the ν_3 region of (a) isotopic SO_3 produced by reaction of ^{16}O (from $^{16}O_3$ photolysis) and mixed isotopic SO_2 species in argon matrix ($S^{16}O_2$, $^{16}OS^{18}O$, $S^{18}O_2/^{16}O_3$/Ar = 1/6/3000 irradiated during 180 min) and (b) isotopic SO_3 produced by reaction of ^{18}O (from $^{18}O_3$ photolysis) and mixed isotopic SO_2 species in argon matrix ($S^{16}O_2$, $^{16}OS^{18}O$, $S^{18}O_2/^{18}O_3$/Ar = 1/6/3000 irradiated during 120 min). Photon flux = 1.14×10^{16} photons cm^{-2} s^{-1}.

Integrated intensities of the isotopic SO_3 species were approximately evaluated despite the overlapping of several bands. The ratio of $S^{666}O_3/S^{668}O_3/S^{886}O_3$ was found to be in agreement with the initial ratio of SO_2 precursors species. In addition to these species spectroscopically identified, features at 1353.6, 1334.3, and 1309.7 cm^{-1} that were previously assigned to $S^{16}O_2$, $^{16}OS^{18}O$, and $S^{18}O_2$ monomers appeared also in both experiments.

A surprising observation is related to the photolysis behavior of the three complexes formed between $S^{16}O_2$, $^{16}OS^{18}O$, and $S^{18}O_2$ with ozone as illustrated in Figure 8. This figure compares

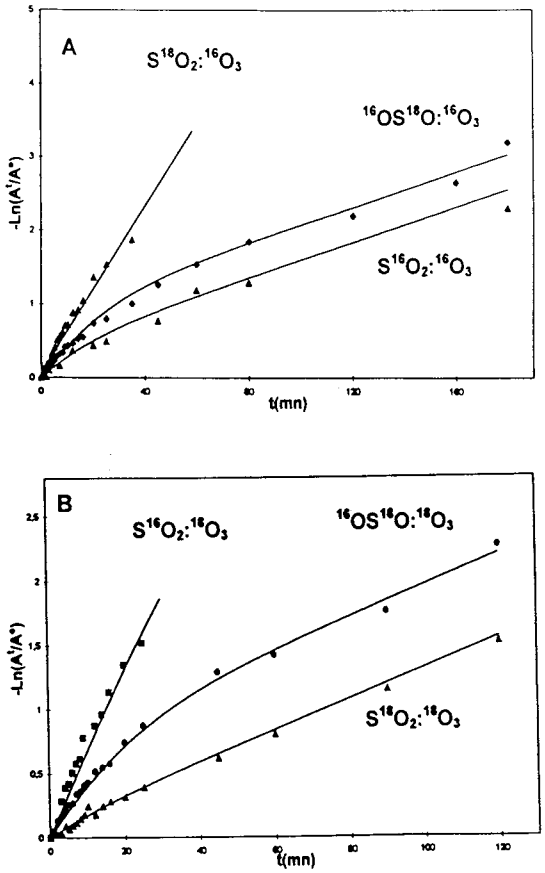

Figure 8. Plots of ln (A^t/A^0) versus irradiation time at 11 K for $S^{16}O_2$:O_3, $^{16}OS^{18}O$:O_3, and $S^{18}O_2$:O_3 decays in argon matrixes. (A) $^{16}O_3$. (B) $^{18}O_3$ (SO_2/O_3/Ar = 1/6/3000).

for the two experiments the kinetic curves of the decrease of all complexes formed between $S^{16}O_2$, $^{16}OS^{18}O$, and $S^{18}O_2$ with natural or isotopic ozone by plotting the quantity ln (A^0/A^t) already introduced versus irradiation time. For the $S^{16}O_2$:$^{16}O_3$ complex (first set of experiments), the intensity of the 1349.5 cm^{-1} band could not accurately be measured due to the overlap

of the $S^{688}O_3$ band, which appears during irradiation. For this species, the intensity measurement of ν_3 of the complex was made from the ν_1 band taking into account the ratio between ν_3/ν_1 absorbances that was found to be 14.3 in the spectroscopic studies described in section 3.2. Several observations can be made: (i) the kinetic decays of $S^{16}O_2$:$^{18}O_3$, $S^{18}O_2$:$^{16}O_3$, and $S^{18}O_2$:$^{18}O_3$ complexes are first-order processes with very different rates, 1.2×10^{-3} s^{-1} for the first two and 2.7×10^{-4} s^{-1} for the latter; (ii) the kinetics of $^{16}OS^{18}O$:$^{16}O_3$, $^{16}OS^{18}O$:$^{18}O_3$, and $S^{16}O_2$:$^{16}O_3$ do not obey a first-order process. The corresponding curves exhibit two distinct phases characterized by two different slopes with apparent rates of 1.2×10^{-3} s^{-1} at $t = 0$ and 2.5×10^{-4} s^{-1} at longer times. The value of 1.2×10^{-3} s^{-1} for $S^{16}O_2$:$^{18}O_3$ and $S^{18}O_2$:$^{16}O_3$ is in agreement with the value found in the $S^{16}O_2$:$^{16}O_3$ and $S^{16}O_2$:$^{18}O_3$ experiments (sections 3.3 and 3.4) if we take into account the diminution of the photon flux.

4. Mechanism of Photooxidation

Formation of SO_3 occurs from two different channels in competition: one by photolysis of the complex SO_2:O_3 and the other one by reaction with a weak yield of the SO_2 monomer with an excited atomic oxygen in the nearest neighbor site. Because of this competition and the weak yield of SO_2 that reacts, the interpretation of the observations is not straightforward.

In the complex, SO_3 is probably directly formed by the transfer of an oxygen atom from ozone to SO_2, and consequently, the photodissociation rates of the different isotopic complexes are expected to be similar. Several examples of formation of simple molecular species from photodissociation of ozone in the charge-transfer band of a molecular complex between ozone and the substrate molecule have been reported in the literature.[34]

Reaction of SO_2 with an oxygen atom is more complex and is now discussed in light of experimental observations with isotopic species that clearly demonstrate the existence of multiple chemical pathways. We have to take into account mainly the following: (i) the formation of $^{16}OS^{18}O$:O_3 and $S^{18}O_2$:O_3 complexes in the photolysis of a $S^{16}O_2$ and $^{18}O_3$ mixture as well as the formation of $S^{688}O_3$ (with a weak yield); (ii) a difference in dissociation rates for the different isotopic variants of the SO_2:O_3 complex in the reaction of mixed isotopic SO_2 with ^{16}O or ^{18}O. We suggest that collisional quenching of $O(^1D)$ by SO_2 arises from the formation of an excited transient species that either fragments as SO_2 and $O(^3P)$ or transforms into SO_3 as

$$SO_2 + O(^1D) \longrightarrow [SO_3]^* \begin{cases} \nearrow SO_2 + O(^3P) \\ \searrow SO_3 \end{cases} \qquad (1)$$

We will discuss below the magnitude of the branching ratio for these elementary reactions, as well as the apparent branching ratio due to secondary processes.

4.1. Nature of the Transient Species. At first sight, the transient species could be the normal trioxide sulfur molecule

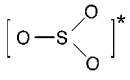

produced in an excited state. In the gas phase, excess energy leads to fragmentation, but in matrixes, the excess energy can dissipate in the matrix phonon bath and the reaction intermediate can be stabilized. Such behavior was observed for intermediate species produced as primary products in the reaction of $O(^1D)$ with N_2 (stabilization of N_2O)[35] or in the reaction of $O(^3P)$ with CH_3Cl (stabilization of $CH_3Cl\cdots O$).[36] Following this interpretation, the deactivation of $[SO_3]^*$ in the matrix should have been similar for the different isotopic species. This is not the case according to our experimental observations for the reaction of mixed isotopic SO_2 with ozone.

Thus, we suggest that the transient species could be one of the isomers of SO_3. From ab initio calculations,[37] four isomers of SO_3 were found: two linear (cis and trans) and two ring isomers. Only the identification of the cis OSOO isomer was previously established from recombination of SO_2 and O in the matrix cage after photolysis of SO_3. Although different isomers of SO_3 can be envisaged as transient species, the formation of a collisional complex between SO_2 and O having the geometry of the S-oxide−cyclic SO_2 monomer[37]

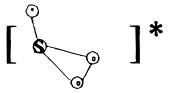

I

appears as the most probable candidate from our observations. This isomer was found to have the lowest energy relative to stable SO_3. According to different quantum chemistry calculations, its energy was estimated to be at $52.57 < E < 58.34$ kcal mol^{-1}.

A careful search of the frequency region where one might expect bands characterizing the transient species was unsuccessful. Transient species formation is probably followed by fast dissociation; very few transient species are present, and their absorption cannot be detected.

4.2. Fragmentation into $SO_2 + O(^3P)$. Because of its energy excess, the intermediate complex dissociates into SO_2 and ground-state atomic oxygen, this fragmentation being in competition with the appearance of stable SO_3.

The identification of a weak yield of $S^{16}O_2$, $^{16}OS^{18}O$, and $^{16}OS^{18}O$:O_3 in the reaction between $S^{16}O_2$ and $^{18}O_3$ is an indication that fragmentation (which is less probable than formation of $S^{668}O_3$ in our experiment) involves two different bond cleavages leading either to $S^{16}O_2$ or to $^{16}OS^{18}O$:

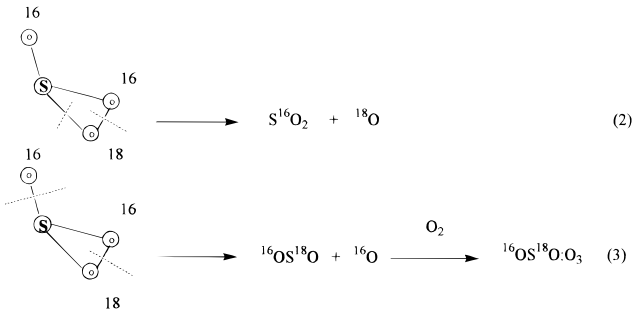

According to the relative orientation of the ground-state atomic oxygen produced by fragmentation, a possible recombination of atomic oxygen with a neighboring oxygen molecule can occur and will lead to reformation of ozone in interaction with $^{16}OS^{18}O$. The formation with a weak yield of $^{16}OS^{18}O$ as compared to production of $^{16}OS^{18}O$:O_3 and $S^{16}O_2$ suggests that the cleavage in reaction 3 is facilitated by the formation of the $^{16}OS^{18}O$:O_3 complex, while the cleavage in reaction 2 leads mainly to SO_2 monomer. Photodissociation of the $^{16}OS^{18}O$:$^{18}O_3$ complex can give the $S^{688}O_3$ species, which was also observed.

SCHEME 1

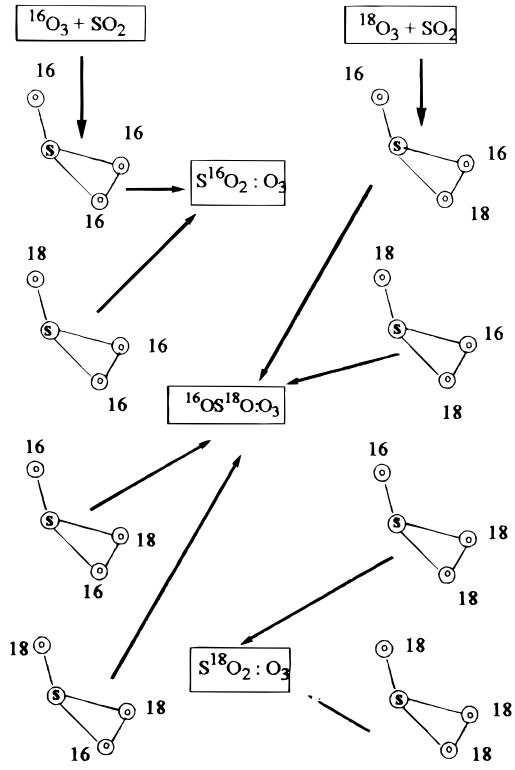

Formation of $S^{688}O_3$ species can also occur from the subsequent reaction of $^{16}OS^{18}O$ with ^{18}O atomic oxygen, and according to eq 1, the formation of $S^{18}O_2$ and $S^{18}O_2$:O_3 is expected to be at trace levels, in agreement with experimental observations.

In the experiments with mixed isotopic SO_2 species, the observed differences in the kinetic rates for the decay of the complexes SO_2:O_3 suggest that the fragmentation pathway of some transient species containing ^{18}O is faster than that for the corresponding normal species leading to complex formation rather than SO_3. Thus the dissociation of initial complexes produced after deposition is compensated by their formation in the $SO_2 + O$ reaction, and their decay rate constant apparently diminishes. The difficult question, however, is why the decay rates of $S^{16}O_2$:$^{18}O_3$ and $S^{18}O_2$:$^{16}O_3$ are faster than the decay rates of $S^{16}O_2$:$^{16}O_3$ and $S^{18}O_2$:$^{18}O_3$. Scheme 1 in which we have assumed that complex formation occurs only by reaction 3 from the transient species could explain this observation. As can be seen, in the $^{16}O_3$ experiment, the $S^{18}O_2$:O_3 complex cannot be formed, and in the $^{18}O_3$ experiment the $S^{16}O_2$:$^{18}O_3$ complex is absent. While in the $^{16}O_3$ experiment, $S^{16}O_2$:$^{16}O_3$ can be produced from $^{18}OS^{16}O^{16}O$ transient species, and in the $^{18}O_3$ experiment, $S^{18}O_2$:$^{18}O_3$ is produced from $^{18}OS^{18}O^{18}O$ and $^{16}OS^{18}O^{18}O$ transient species. Consequently, the kinetic rate of 1.2×10^{-3} s^{-1} observed for the decrease of $S^{16}O_2$:$^{18}O_3$ or $S^{18}O_2$:$^{16}O_3$ species corresponds only to the decrease of initial complexes without additional formation from the reaction $SO_2 + O$. From the value of 1.2×10^{-3} s^{-1} (obtained with a photon flux of 1.14×10^{16} photons cm^{-2} s^{-1}), the initial kinetic rate for the dissociation of the complex $S^{16}O_2$:$^{16}O_3$ is expected to be 4.2×10^{-3} s^{-1} for a photon flux of 4.2×10^{16} photons cm^{-2} s^{-1}. This value was observed in the experiment using natural abundance SO_2 and ozone, and this shows that subsequent formation of $S^{16}O_2$:$^{16}O_3$ from the $S^{16}O_2 + {}^{16}O$ reaction is a minor channel in regard to the formation of natural $S^{666}O_3$ in this experiment.

4.3. Formation of SO_3. At first chemical insight, the stable SO_3 species could originate from the rearrangement or stabilization of the transient species **I**. However, this assumption cannot explain why ^{18}O-containing transient species lead to different yields of the isotopic SO_2:O_3 complexes, since cleavage of the $S^{18}O$ or $S^{16}O$ bonds is expected to be only slightly different. Consequently, from observed isotopic effects, we suggest that SO_3 is formed from **I** by a tunneling effect as observed recently for the isomerization of ClON into ClNO in argon and nitrogen matrixes.[38] The kinetics of the spontaneous conversion of ClON into ClNO showed that the rate of this process depends on the nature of the isotopic species. For example, in nitrogen matrix the destruction rate for the $Cl^{16}O^{14}N$ species was 1 order of magnitude larger than for the $Cl^{18}O^{15}N$ molecule. A tunneling effect for the isomerization of $[SO_3]^*$ into SO_3 can explain the different rates observed for the three isotopic SO_2:O_3 complexes. For the $S^{666}O_3$* transient species, conversion into normal SO_3 is fast, and photodissociation leading to the SO_2:O_3 complex is negligible. For $S^{668}O_3$* and $S^{888}O_3$* transient species, conversion is slower, and fragmentation becomes preponderant.

4.4. Kinetic Curves of the Complex in Mixed Isotopic SO_2 Experiments. Taking into account the assumptions suggested above concerning competition between fragmentation of the transient species and conversion into normal SO_3 by a tunneling effect, we have tested a simplified model to fit the experimental kinetic curves of the $S^{16}O_2$:$^{16}O_3$, $^{16}OS^{18}O$:$^{16}O_3$, $S^{18}O_2$:$^{18}O_3$, and $^{16}OS^{18}O$:$^{18}O_3$ complexes formed by reaction of $SO_2 + O$ (resulting from the O_3 photolysis) in the mixed isotopic SO_2 experiments.

A model was built based on the following simplifying hypotheses: (i) only a weak fraction X of SO_2 and O_3 (almost in equal abundance) molecules in neighboring sites can lead to SO_3* transient formation with a rate depending on the effective O_3 photodissociation rate k_1, (ii) there exists a stationary state for the transient species, and (iii) only reaction 3 for the fragmentation process of the transient species is considered

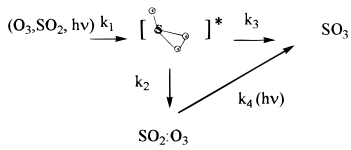

(4)

where k_1 is the rate constant for the formation of $[SO_3]^*$; k_2 is the rate constant for the fragmentation of $[SO_3]^*$ leading to the formation of the SO_2:O_3 complex; k_3 is the rate constant of the interconversion of $[SO_3]^*$ into SO_3 by tunneling; and k_4 is the rate constant of the SO_2:O_3 complex for the photodissociation of the SO_2:O_3 complex.

Thus the kinetic equations that must be considered are

$$\frac{d[SO_3]^*}{dt} = k_1[O_3, SO_2, h\nu] - k_2[SO_3^*] - k_3[SO_3^*] = 0 \quad (5)$$

$$\frac{d[SO_2{:}O_3]}{dt} = k_2[SO_3^*] - k_4[SO_2{:}O_3] \quad (6)$$

From eq 5 and writing $[O_3, SO_2, h\nu] = X = X^0 \exp^{-k_1 t}$, eq 6 can be written:

$$\frac{d[SO_2{:}O_3]}{dt} = -k_4[SO_2{:}O_3] - \frac{k_2 k_1 X^0 \exp^{-k_1 t}}{k_2 + k_3} \quad (7)$$

Integration of eq 7 gives the concentration of the $[SO_2$:$O_3]$ complex at each time t, and writing $[SO_2{:}O_3]_{(t=0)} = C^0$, one

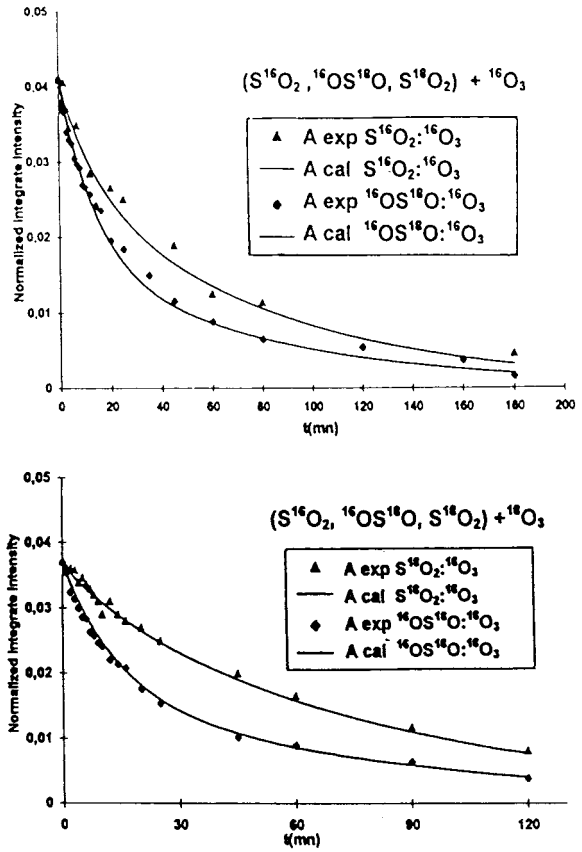

Figure 9. Comparison of experimental results and calculated from eq 9 kinetic curves of the SO_2:O_3 complex disappearance using normalized integrated intensities of the ν_3 SO_2 absorption features and $k_1 = 2 \times 10^{-4}$, $k_2 = 1.2 \times 10^{-4}$, $k_4 = 1.2 \times 10^{-3}$, $k_3 = 4.8 \times 10^{-4}$ ($^{16}OS^{18}O$:$^{16}O_3$), 4.2×10^{-4} ($^{16}OS^{18}O$:$^{18}O_3$), 5.0×10^{-4} ($S^{16}O_2$:$^{16}O_3$), and 8×10^{-6} s^{-1} ($S^{18}O_2$:$^{18}O_3$).

gets (using Mathlab) the following:

$$[SO_2{:}O_3]_{(t)} = \{\exp^{-k_4 t}[k_2k_4C^0 + k_3k_4C^0 - k_1k_2X^0 - k_1k_2C^0 - k_1k_3C^0] + k_1k_2X^0 \exp^{-k_1 t}\}/\{k_3k_4 + k_2k_4 - k_1k_3 - k_1k_2\} \quad (8)$$

The k_4 rate constant is known (1.2×10^{-3} s^{-1}) from our experimental results as well as C^0, the initial complex concentration, which is proportional to the integrated intensity of complexed SO_2 in the region of ν_3. Relative rate constants k_1 and k_2 were estimated from the disparition curve of ozone and from the formation curve of SO_2 resulting from the dissociation of the transient species and the production of "free" SO_2 (band at 1352.4 cm^{-1} for $S^{16}O_2$). The quantities X^0 were chosen to be 0.17 from the measurement of the integrated intensity of the ν_3 of O_3 (in arbitrary absorbance units used to normalize all our measurements).

Fitting the kinetic curves of $^{16}OS^{18}O$:$^{6}O_3$, $S^{16}O_2$:$^{16}O_3$ and $S^{18}O_2$:$^{18}O_3$, and $^{16}OS^{18}O$:$^{18}O_3$ was made keeping the same values of all parameters except the rate constant k_3 of the tunneling process, the only process that is expected to vary from one isotopic SO_2 species to the other. Figure 9 compares experimental results with fitting curves calculated from eq 8. As can be seen, the fitting is satisfactory with values of k_3, which were found to be 4.2×10^{-4} ($^{16}OS^{18}O$:$^{18}O_3$), 8×10^{-6} ($S^{18}O_2$:$^{18}O_3$), 5×10^{-4} ($S^{16}O_2$:$^{16}O_3$), and 4.8×10^{-4} s^{-1} ($^{16}OS^{18}O$:$^{16}O_3$). This confirms the competition between fragmentation that leads to the formation of SO_2:O_3 and conversion of the transient species

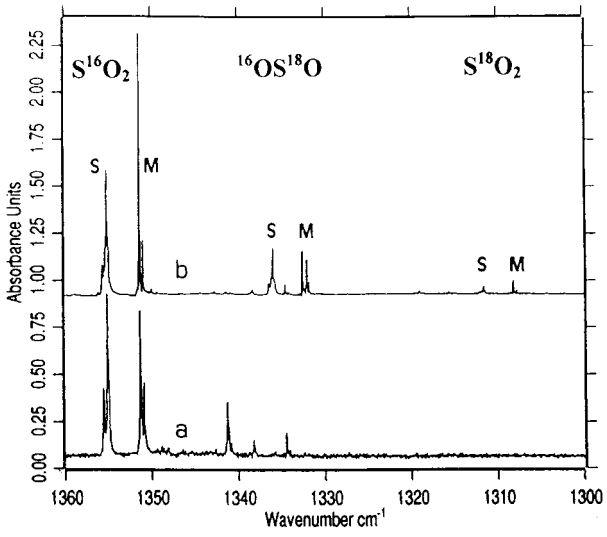

Figure 10. Comparison in the ν_3 region of SO_2 for spectra recorded at 11 K in the following conditions. (a) $S^{16}O_2$ and $^{18}O_3$ mixture diluted in argon in the same sample. (b) $S^{16}O_2$ and $^{18}O_3$ mixture irradiated at room temperature during several hours with a medium-pressure mercury lamp and then diluted in argon ($SO_2/O_3/Ar = 1/1/3000$). S and M, SO_2 in stable and metastable sites, respectively.

by tunneling to stable SO_3. According to the origin of formed complexes (see Scheme 1), calculated k_3 values indicate that the tunneling rate constant of $^{18}OS^{18}O^{18}O$ species is the lowest. Tunneling rate constants of $^{18}OS^{16}O^{16}O$, $^{16}OS^{16}O^{18}O$, and $^{16}OS^{18}O^{18}O$ species are expected to be lower than that of the normal $^{16}OS^{16}O^{16}O$ species since, in the reaction of pure $S^{16}O_2$ with $^{16}O_3$ or $^{18}O_3$, the formation of the $S^{16}O_2$:O_3 complex by $SO_2 + O$ is negligible. As a matter of fact, fitting the experimental SO_2:O_3 decay curve with our simplified model led to a value of 4.2×10^{-3} s^{-1} for k_3, a value 1 order of magnitude larger than that calculated from the decay of $^{16}OS^{18}O$:O_3.

5. Implication to Atmospheric Chemistry

The results obtained in the present work demonstrate that in the gas phase the conversion of SO_2 into SO_3 by ozone would proceed only through the intermediate complex formed between SO_2 and ozone, a minor channel, because relatively few complex species are expected to exist in the gas phase. Reaction of $O(^1D)$ with SO_2, which leads to SO_3 in the matrix by tunneling, is not expected in the gas phase, but our experiments provide evidence that quenching of $O(^1D)$ by collision with SO_2 could occur in the gas phase through the formation of an excited intermediate complex assumed to be **I** on a bound singlet potential surface having an intersection with the triplet state and then relaxing either to $SO_2 + O$ or to SO_3 with a very small yield.

Although we have no direct evidence for this transient species, its formation in the gas phase as in the matrix could be evidenced by the observation of isotopic SO_2 species formed from $S^{16}O_2$ and $^{18}O(^1D)$ interactions. With this in mind, we have irradiated at room temperature a gaseous mixture of $S^{16}O_2$ and $^{18}O_3$ (10 Torr of each reactant) with a medium-pressure mercury lamp and used the matrix technique as a diagnostic of the products formed in the gas phase. As illustrated in Figure 10, we have observed after irradiation of the gaseous mixture the signatures of $^{16}OS^{18}O$ and $S^{18}O_2$, whereas these species were not observed by thermal isotopic exchange in a parallel blank experiment (without photolysis).

The reaction scheme involved in Ar, the photolysis experiments of the O_3/SO_2 system and leading to SO_3, could be

operative on planetary ice containing adsorbed SO_2 and ozone species and subject to solar irradiation. The present study provides a base for future experiments to simulate such conditions.

Acknowledgment. We thank Dr. Claude Camy-Peyret, Director of LPMA, for reading and improving the manuscript.

References and Notes

(1) Möller, D. *Atmos. Environ.* **1980**, *14*, 1067.
(2) Stockwell, W. R.; Calvert, J. G. *Atmos. Environ.* **1983**, *17*, 2231.
(3) *Acid Precipitation Series*; Calvert, J. G., Teasley, J. I., Eds.; Butterworths: Boston, 1984; Vol. 3.
(4) *The Chemistry of Acid Rain*; Johnson, R. W., Gordon, G. E., Eds.; American Chemical Society: Washington, DC, 1987.
(5) Warneck, P. *Chemistry of the Natural Atmosphere*; Academic Press: New York, 1988.
(6) Sodeau, J. R.; Lee, E. K. C. *J. Phys. Chem.* **1980**, *84*, 3358.
(7) Green, M.; Lee, E. K. C. *J. Phys. Chem.* **1986**, *90*, 6470.
(8) Schriver-Mazzuoli, L.; Carrere, D.; Schriver, A.; Jaeger, K. *Chem. Phys. Lett.* **1991**, *181*, 505.
(9) Nahir, T. M.; Dawson, G. A. *J. Atmos. Chem.* **1987**, *5*, 373.
(10) Calvert, J. G.; Stockwell, W. R. *Environ. Sci. Technol.* **1983**, *17*, 428.
(11) Lee, Y. Y.; Kao, W. C. *J. Phys. Chem.* **1990**, *94*, 4535.
(12) Schriver-Mazzuoli, L.; Schriver A.; Lugez, C.; Perrin, A.; Camy-Peyret, C.; Flaud, J. M. *J. Mol. Spectrosc.* **1996**, *85*, 175.
(13) Brosset, P.; Dahoo, R.; Gauthier-Roy, B.; Abouaf-Marguin, L.; Lakhlifi, A. *Chem. Phys.* **1993**, *172*, 315.
(14) Michelsen, H. A.; Salawitgh, R. J.; Wennberg, P. O.; Anderson, J. G. *Geophys. Res. Lett.* **1994**, *21*, 2227.
(15) Benderskii, A. V.; Wight, C. A. *J. Chem. Phys.* **1994**, *101*, 292.
(16) Bahou, M.; Schriver-Mazzuoli, L.; Schriver, A. *J. Chem. Phys.* **1999**, *110*, 8636.
(17) Schriver-Mazzuoli, L.; Schriver, A.; Wierzejewska-Hnat, M. *Chem. Phys.* **1995**, *199*, 227.
(18) Chen, L. S.; Lee, C. I.; Lee, Y. P. *J. Chem. Phys.* **1996**, *105*, 9457.
(19) Heicklen K.; Kelly, N.; Partymiller, K. *Rev. Chem. Int.* **1980**, *3*, 315.
(20) James, F. C.; Kerr, J. A.; Simons, J. P. *Chem. Phys. Lett.* **1974**, *25*, 431.
(21) Sidebottom, H. W.; Badcok, C. C.; Calvert, J. G.; Reinhardt, G. E.; Rabe, B. R.; Damon, E. K. *J. Am. Chem. Soc.* **1971**, *93*, 2587.
(22) Schriver, A.; Schriver-Mazzuoli, L.; Perchard, J. P. *J. Mol. Spectrosc.* **1988**, *127*, 126.
(23) Nord, L. *J. Mol. Struct.* **1982**, *96*, 30.
(24) Wierzejewska-Hnat, M.; Mielke, Z.; Wieczorek, R.; Latajka, Z. *Chem. Phys.* **1998**, *228*, 26.
(25) Li, S.; Li, Y. S. *J. Mol. Struct.* **1993**, *301*, 21.
(26) *Chemistry and Physics of Matrix Isolated Species*; Andrews, L., Moskovits, M., Eds.; North-Holland: New York, 1989; p 42.
(27) Lugez, C.; Schriver, A.; Levant, R.; Schriver-Mazzuoli, L. *Chem. Phys.* **1994**, *181*, 137.
(28) Schriver-Mazzuoli, L. Unpublished results.
(29) Givan, A.; Larsen, L. A.; Loewenschuss, A.; Nielsen, C. J. *J. Chem. Soc., Faraday Trans.* **1998**, *94*, 827.
(30) Schriver-Mazzuoli, L.; Gauthier-Roy, B.; Carrere, D.; Schriver, A.; Abouaf-Marguin, L. *Chem. Phys.* **1992**, *163*, 357.
(31) Pettersen, M. V.; Schriver-Mazzuoli, L.; Schriver, A.; Chaquin, P.; Lasson, E. *Chem. Phys.* **1996**, *204*, 115.
(32) *Molecular Spectroscopy: Modern Research*; Rao, K. N., Ed.; Academic Press: New York, 1985; Vol. 3.
(33) Kugel, R.; Taube, H. *J. Phys. Chem.* **1975**, *79*, 2130.
(34) Schriver-Mazzuoli, L. In *Molecular Complexes in Earth's Planetary, Cometary and Interstellar Atmospheres*; Vigassin, A. A., Slanina, Z., Eds.; World Scientific: River Edge, NJ, 1998; pp 194−237.
(35) Bahou, M.; Schriver-Mazzuoli, L.; Camy-Peyret, C.; Schriver, A. *J. Chem. Phys.* **1998**, *108*, 6884.
(36) Schriver-Mazzuoli, L.; Schriver, A.; Hannachi, Y. *J. Phys. Chem.* **1998**, *102*, 10221.
(37) Jou, S. H.; Shen, M. S.; Yu, C. H.; Lee, Y. P. *J. Chem. Phys.* **1996**, *104*, 5745.
(38) Hallou, A.; Schriver-Mazzuoli, L.; Schriver, A.; Chaquin, P. *Chem. Phys.* **1998**, *237*, 251.